Journal of Computational Physics **171,** 182–200 (2001)
doi:10.1006/jcph.2001.6781, available online at http://www.idealibrary.com on IDEAL®

A New Code for Electrostatic Simulation by Numerical Integration of the Vlasov and Ampère Equations Using MacCormack's Method

Richard B. Horne and Mervyn P. Freeman

British Antarctic Survey, Natural Environment Research Council, Madingley Road, Cambridge CB3OET, United Kingdom
E-mail: R.Horne@bas.ac.uk

Received August 11, 1998; revised March 5, 2001

We present a new simulation code for electrostatic waves in one dimension which uses the Vlasov equation to integrate the distribution function and Ampère's equation to integrate the electric field forward in time. Previous Vlasov codes used the Vlasov and Poisson equations. Using Ampère's equation has two advantages. First, boundary conditions do not have to be set on the electric field. Second, it forms a logical basis for an electromagnetic code since the time integration of the electric and magnetic fields is treated in a similar way. MacCormack's method is used to integrate the Vlasov equation, which was found to be easy to implement and reliable. A stability analysis is presented for the MacCormack scheme applied to the Vlasov equation. Conditions for stability are more stringent than the simple Courant–Friedrich's–Lewy (CFL) conditions for the spatial and velocity grids. We provide a simple linear function which when combined with the CFL conditions should ensure stability. Simulation results for Landau damping are in excellent agreement with numerical solutions of the linear dispersion relation for a wide range of wavelengths. The code is also able to retain phase memory as demonstrated by the recurrence effect and reproduce the effects of particle trapping. The use of Ampère's equation enables standing and traveling waves to be produced depending on whether the current is zero or non-zero, respectively. In simulations where the initial current is non-zero and Maxwell's equations are satisfied initially, additional standing waves may be set up, which could be important when the coupling of wave fields from a transmitter to a plasma is considered.

0021-9991/01 $35.00

INTRODUCTION

Numerical simulations have become an increasingly important tool to study complex problems in space plasma physics. The kinetic theory of collisionless space plasmas is described by the set of Vlasov–Maxwell equations. There are two methods commonly used to solve these equations: one is the particle-in-cell (PIC) method and the other is known as the Vlasov simulation method [17]. In both methods there are three dependent variables, the particle distribution function $f(\mathbf{r}, \mathbf{v}, t)$ and the electromagnetic fields $\mathbf{E}(\mathbf{r}, t)$ and $\mathbf{B}(\mathbf{r}, t)$. There are three independent variables, space $\mathbf{r}$, velocity $\mathbf{v}$, and time t. The PIC method is the one most widely used and is in effect a mixed Lagrangian–Eulerian method. Here f is represented by many test particles or super particles. By Lagrangian integration along the particle trajectories using the discretized form of the particle equations of motion, f is reconstructed at a later time by summing up these super particles in each cell of an Eulerian grid. The current $J(\mathbf{r}, t)$ and charge density $\rho(\mathbf{r}, t)$ are obtained by integrating f over $\mathbf{v}$, and are used to step $\mathbf{E}$ and $\mathbf{B}$ forward by solving Maxwell's equations on the discrete Eulerian grid.

In the Vlasov simulation method the particle distribution function f is defined on a grid in phase $(\mathbf{r}, \mathbf{v})$ space. Several methods have been used to solve the Vlasov–Maxwell equations including finite difference [3], semi-Lagrangian [6], and spectral methods [11]. Hybrid techniques have also been used [8, 19] which are mixed Lagrangian–Eulerian methods like the PIC method. However, the particles are used only to provide information on how the distribution function is carried across phase space. The distribution function is integrated forward in time using Liouville's theorem which states that for a given particle species f is constant along the particle trajectory in phase space.

The fact that one super particle represents many real particles in a PIC code leads to two disadvantages: First, particle codes have relatively high numerical noise, and second, the results are scaled by the unphysical mass and charge of the super particles. High numerical noise means that very often simulations have to be set up with unrealistic input values in order to obtain results above the noise level. This may not always pertain to observations. In addition, numerical noise causes unwanted numerical particle diffusion [21]. In contrast, Vlasov codes have very low noise levels and are not subject to mass scaling. However, Vlasov codes are subject to problems which result from filamentation in which fine structure develops in the distribution function. The fine structure develops with time until it becomes comparable to the grid spacing in which case numerical diffusion may ensue and in some cases the simulation may fail. Filamentation has been a particularly difficult problem to overcome, and is one reason why the use of PIC codes has become so widespread. However, a solution to the filamentation problem was found by Klimas [14] and demonstrated by Klimas and Farrell [15]. This has stimulated the development of new Vlasov codes. The recurrence effect [6] is another limitation of the Vlasov codes that is related to filamentation but is unphysical. Recurrence is a problem for simulations where the wave field is decaying, but should not present a problem in simulations where the waves are growing since the electric field perturbs the ballistic trajectories and may cause trapping in certain velocity ranges. Vlasov codes have also been difficult to extend to more than one dimension due to the large requirements for computer memory and speed. With the development of massively parallel computers this will become less of a problem.

Several techniques have been developed to integrate the Vlasov equation. Gazdag [10] used an accurate space derivative method which was accurate to the third order for one dimension in real space and two dimensions in velocity space (1d2v). This was applied to

Bernstein waves propagating across the magnetic field. Cheng and Knorr [6] introduced a splitting scheme in which the Vlasov equation is broken down into two coupled equations and integrated for half a time step in space and then half a time step in velocity space. They applied this to study linear and nonlinear Landau damping of Langmuir waves in one dimension. It has since been used by other authors in applications to double layers [4]. Other methods, using Fourier transforms, have also been demonstrated [15].

One feature common to all these previous studies is that they solve Vlasov's equation with Poisson's equation. In this paper we present a new technique which solves Vlasov's equation with Ampère's law. By solving these two equations we can calculate the time evolution of the electric field directly without having to apply spatial boundary conditions to the electric field. This should yield the same physical results for electrostatic waves [16], but the method should be extendable to electromagnetic waves as well. We demonstrate that the method agrees with the results of Landau damping for both standing and traveling waves and can also reproduce the effects of nonlinear trapping. The use of Ampère's equation enables both propagating and traveling wave solutions for periodic boundary conditions.

THE VLASOV–MAXWELL EQUATIONS

We consider the set of Vlasov–Maxwell equations for 1D in space, and 1D in velocity space, with no external magnetic field. We consider only electrostatic waves where the induced magnetic field is so small it can be neglected. We integrate the Vlasov equation

$$\frac{\partial f_\sigma}{\partial t} = -v_x \frac{\partial f_\sigma}{\partial x} - \frac{q_\sigma}{m_\sigma} E_x \frac{\partial f_\sigma}{\partial v_x}, \tag{1}$$

together with Ampère's law

$$\frac{\partial E_{x,int}}{\partial t} = -c^2 \mu_\circ J_{x,int}, \tag{2}$$

and check that Poisson's equation is satisfied

$$\frac{\partial E_{x,int}}{\partial x} = \frac{\rho_{int}}{\epsilon_\circ}, \tag{3}$$

where $E_x(x,t) = E_{x,int} + E_{x,ext}$ is the sum of the internal and external electric fields, and $\rho_{int}(x,t)$ and $J_{x,int}(x,t)$ are the charge and current densities given by

$$\rho_{int}(x,t) = \sum_\sigma q_\sigma \int f_\sigma(x, v_x, t)\, dv_x, \tag{4}$$

$$J_{x,int}(x,t) = \sum_\sigma q_\sigma \int v_x\, f_\sigma(x, v_x, t)\, dv_x, \tag{5}$$

where the summation is over all ion and electron species in the plasma. Here we consider the ions to be H^+ and to form a fixed neutralizing background with constant phase space density. We only consider electron dynamics. This is reasonable for time scales of the order of $\sqrt{m_i/m_e} \approx 43$ electron plasma periods or under conditions where the ion dynamics is not important. The external electric field, E_{ext}, satisfies equations analogous to Eq. (2) and (3) but with $E_{x,int}$, $J_{x,int}$, and ρ_{int} replaced by $E_{x,ext}$, $J_{x,ext}$, and ρ_{ext}. Note that $J_{x,ext}$ and

ρ_{ext} are not determined by the distribution function since they are external. From now on we drop the subscript x on the one-dimensional vector quantities and the subscripts int and ext since we shall not consider applied external fields.

THE INTEGRATION METHOD

At time $t = 0$ we specify $f(x, v)$ and $E(x)$ and calculate $\rho(x)$ and $J(x)$ from Eqs. (4) and (5). We integrate (1) and (2) to get $f(x, v)$ and $E(x)$ at the new time step and then use the new f in Eqs. (4) and (5) to calculate $\rho(x)$ and $J(x)$. We then repeat the cycle for the required number of time steps. At each time step we check that Eq. (3) is satisfied and that $\int f dx dv$ is conserved.

Specifically, we use MacCormack's integration method (e.g., [1]) for the Vlasov equation. This has the advantage that it does not require explicit calculation of second derivatives and yet it is accurate to second order. It is therefore easier to implement than other methods, such as the Lax–Wendroff method, used in other space plasma simulation codes. Writing $f^n_{i,j}$ as the distribution function at position $x = i\Delta x$ with velocity $v_x = j\Delta v$ at time $t = n\Delta t$, we can estimate f at the $n + 1$ time step to second order by the Taylor series

$$f^{n+1}_{i,j} = f^n_{i,j} + \Delta t \frac{\partial f}{\partial t}\bigg|^n_{i,j} + \frac{\Delta t^2}{2}\frac{\partial^2 f}{\partial t^2}\bigg|^n_{i,j} + \cdots; \tag{6}$$

similarly we have

$$\frac{\partial f}{\partial t}\bigg|^{n+1}_{i,j} = \frac{\partial f}{\partial t}\bigg|^n_{i,j} + \Delta t \frac{\partial^2 f}{\partial t^2}\bigg|^n_{i,j} + \cdots. \tag{7}$$

Eliminating $\frac{\partial^2 f}{\partial t^2}|^n_{i,j}$ we obtain

$$f^{n+1}_{i,j} = f^n_{i,j} + \frac{\Delta t}{2}\left[\frac{\partial f}{\partial t}\bigg|^{n+1}_{i,j} + \frac{\partial f}{\partial t}\bigg|^n_{i,j}\right] + O(\Delta t^3). \tag{8}$$

In the MacCormack method we calculate $\frac{\partial f}{\partial t}|^n$ and $\frac{\partial f}{\partial t}|^{n+1}$ by finite difference as follows: The first step is to use forward difference in space (i) and velocity (j) to obtain

$$\left(\frac{\partial f}{\partial t}\right)^n_{i,j} = -v_j\left[\frac{f^n_{i+1,j} - f^n_{i,j}}{\Delta x}\right] - \frac{q}{m}E^{n+1/2}_i\left[\frac{f^n_{i,j+1} - f^n_{i,j}}{\Delta v}\right]. \tag{9}$$

The second step is to predict $f_{i,j}$ at the next time step using a first-order Taylor series

$$\bar{f}^{n+1}_{i,j} = f^n_{i,j} + \Delta t\left(\frac{\partial f}{\partial t}\right)^n_{i,j}. \tag{10}$$

The third step is to estimate the time derivative of $\bar{f}_{i,j}$ using backward difference,

$$\left(\overline{\frac{\partial f}{\partial t}}\right)^{n+1}_{i,j} = -v_j\left[\frac{\bar{f}^{n+1}_{i,j} - \bar{f}^{n+1}_{i-1,j}}{\Delta x}\right] - \frac{q}{m}E^{n+1/2}_i\left[\frac{\bar{f}^{n+1}_{i,j} - \bar{f}^{n+1}_{i,j-1}}{\Delta v}\right]. \tag{11}$$

Finally f is integrated forward in time by substituting (9) and (11) into (8) where $(\overline{\frac{\partial f}{\partial t}})_{i,j}^{n+1}$ is an estimate of $(\frac{\partial f}{\partial t})_{i,j}^{n+1}$.

Since the average time derivative is taken between t and $t + \Delta t$ using forward and backward difference it can be shown that $f_{i,j}^{n+1}$ is accurate to second order in space and time [1]. Boundary conditions are applied to interpolate the new f onto the outermost grid cells which cannot be calculated from Eq. (8). The interpolation region is only one grid cell wide in contrast to two grid cells wide for second order methods.

To calculate Eqs. (9) and (11) the electric field must be integrated before the Vlasov equation. Since the current J at time t is known we use a second-order central difference method to integrate the electric field

$$E_i^{n+1} = 2\Delta t \left(\frac{\partial E}{\partial t}\right)_i^n + E_i^{n-1} = -2\Delta t c^2 \mu_\circ J_i^n + E_i^{n-1} \tag{12}$$

to obtain

$$E_i^{n+1/2} = \frac{1}{2}\left(E_i^n + E_i^{n+1}\right), \tag{13}$$

where E and J refer to the internal electric field and current, respectively. Since the current is obtained from an integration over velocity space it does not depend on grid cells outside the simulation box. Thus boundary conditions do not have to be set on the electric field. This is an advantage over using Poisson's equation for finding the electric field.

STABILITY ANALYSIS

We now present a stability analysis for our Vlasov simulation code using the MacCormack scheme. Substituting (6), (7), (8), and (10) into (9) we obtain an expression for f^{n+1} in terms of f^n and terms involving v_j, v_{j-1}, E_i^n, and E_{i-1}^{n+1}. By expanding all terms involving $i-1$, $j-1$, etc. in Taylor series and neglecting terms of order $(\Delta t)^3$ and above, the resulting expression can be written back in an analytical form. The analytical form is exactly the same as that obtained by expanding the Vlasov equation in a Taylor series neglecting third and higher order terms given by

$$\begin{aligned} f(t+\Delta t) = {} & f(t) - v\Delta t\frac{\partial f}{\partial x} + v^2\frac{\Delta t^2}{2}\frac{\partial^2 f}{\partial x^2} - \frac{q}{m}E\Delta t\frac{\partial f}{\partial v} + \frac{q^2}{m^2}E^2\frac{\Delta t^2}{2}\frac{\partial^2 f}{\partial v^2} \\ & + \frac{q}{m}\frac{\Delta t^2}{2}\left(v\frac{\partial E}{\partial x} - \frac{\partial E}{\partial t}\right)\frac{\partial f}{\partial v} + \frac{q}{m}Ev\Delta t^2\frac{\partial^2 f}{\partial x \partial v} + \frac{q}{m}E\frac{\Delta t^2}{2}\frac{\partial f}{\partial x}. \end{aligned} \tag{14}$$

Note here that the last three terms express the coupling between convection in real space and convection in velocity space. They are important for the stability calculations below. We also note that the difference between using $E^{n+1/2}$ as opposed to E^n in (9) and E^{n+1} in (11) is negligible since the difference is on the order of $(\Delta t)^3$. This has been checked in our simulations.

Assuming that f varies as $\exp(ikx)\exp(ik_v v)$, then E varies as $\exp(ikx)$, and we obtain an amplification factor, g, for the MacCormack method given by

$$\begin{aligned} g = \frac{f_{i,j}^{n+1}}{f_{i,j}^n} = {} & 1 - ib_j\sin(\phi) + b_i^2(\cos\phi - 1) - ia_i\sin(\psi) + a_i(\cos\psi - 1) \\ & + \frac{1}{2}a_i b_i[\cos\phi + \cos\psi - 2 - \cos(2\phi - \psi) + \cos 2\phi] \end{aligned}$$

$$+ i\frac{1}{2}a_i b_i[\sin\phi + \sin\psi + \sin(2\phi - \psi) - \sin 2\phi]$$
$$- \frac{1}{2}a_i(b_j - b_1)[\cos(\phi - \psi) - \cos\phi + i\sin(\phi - \psi) + i\sin\psi], \quad (15)$$

where

$$a_i = \frac{\Delta t}{\Delta v}\frac{q_e}{m_e}E_i^{n+1/2} \quad (16)$$

and

$$b_j = \frac{\Delta t}{\Delta x}v_j, \quad (17)$$

and $\phi = k\Delta x$ and $\psi = k_v\Delta v$. For stability we require $|g|^2 \leq 1$. In the limit $E = 0$, which is the free-streaming case, we obtain

$$\Delta t \leq \frac{\Delta x}{v_j} \quad (18)$$

which is the well-known Courant–Friedrich's–Lewy (CFL) condition for stability. Figure 1a shows the variation of $|g|$ with $k\Delta x$ for a Courant factor, $C_F = v_j\Delta t/\Delta x = 0.8$. It shows that short wavelength waves are heavily damped. In the limit, $v_j = 0$, where the advection term is neglected, we obtain

$$\Delta t \leq \frac{m_e}{q_e}\frac{\Delta v}{E_i^{n+1/2}}, \quad (19)$$

which, by analogy, represents the condition for numerical stability on the velocity grid. It effectively says that in time Δt information must not propagate across more than one velocity cell. In the MacCormack scheme used here the stability requirement is more stringent than that given by the CFL condition since the integration involves extra terms such as the $\partial^2 f/\partial x\partial v$ term. Figure 1b shows the computed values of $|g|$ for a range of a and b between 0 and 1 in steps of 0.04. At each value of a and b, $|g|$ has been computed for ψ and ϕ varying between 0 and π in steps of 5°. Contours of the marginally unstable values of g between 1.02 and 1.10 are shown by the solid lines and lie outside the dashed line corresponding to $a = 1 - b$. Inside the dashed line we have $|g| < 1$ and the scheme is stable.

Thus, satisfying Eqs. (18) and (19) is not sufficient for stability since it is still possible to have a range of $a \leq 1$ and $b \leq 1$ where $|g| > 1$; for example, $a = 0.8$ and $b = 0.8$. In the MacCormack scheme used here stability also requires, to a good approximation,

$$a \leq 1 - b. \quad (20)$$

In all our simulations we ensure that conditions (18), (19), and (20) are satisfied, where v_j is replaced with the maximum grid velocity v_{cut} and $E_i^{n+1/2}$ is replaced with the maximum electric field E_{max}. The time step is also multiplied by a Courant factor $C_F = 0.8$ to ensure stability.

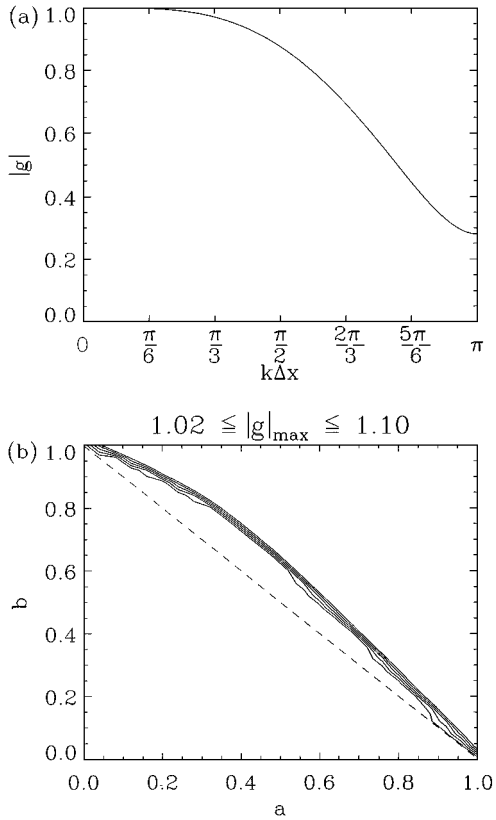

FIG. 1. Stability of the MacCormack method for integrating the Vlasov equation. (a) The amplification factor, $|g|$, versus normalized wavenumber, $k\Delta x$, for the free-streaming Vlasov equation and a Courant factor, $C_F = 0.8$. (b) The amplification factor, $|g|$, versus the velocity space Courant factor, a, and the real space Courant factor, b, for the full Vlasov equation. Cases of marginal instability $1.02 \leq |g| \leq 1.10$ are shown by the solid lines. The dashed line indicates $a = 1 - b$, which approximately separates the stable ($|g| \leq 1$) and unstable ($|g| > 1$) regions.

CURRENT INTEGRATION

It is important to calculate the current accurately in order to step the electric field forward in time. This involves an integration over velocity space as defined in Eq. (5). We have tried three different integration methods. The first is a simple summation over velocity space from negative to positive velocities, the second is a three point Simpson method, and the third is a summation in pairs. The "in pairs" method calculates the function at $vf(v)$ and $-vf(-v)$, so that they should be of the same order of magnitude but opposite in sign, and forms the sum. This is repeated for other values of v until the whole range is covered.

We have performed a series of integration tests by calculating, for each of the three integration methods, the current of a drifting Maxwellian distribution at various drift velocities. The distribution function is defined by

$$f(x, v_x) = \frac{n_e(x)}{\pi^{1/2}\alpha_e} \exp\left[-(v_x - v_d)^2/\alpha_e^2\right] \delta(v_y)\delta(v_z), \tag{21}$$

where for each component $n_e(x)$ is the electron number density in m^{-3}, v_d is the drift

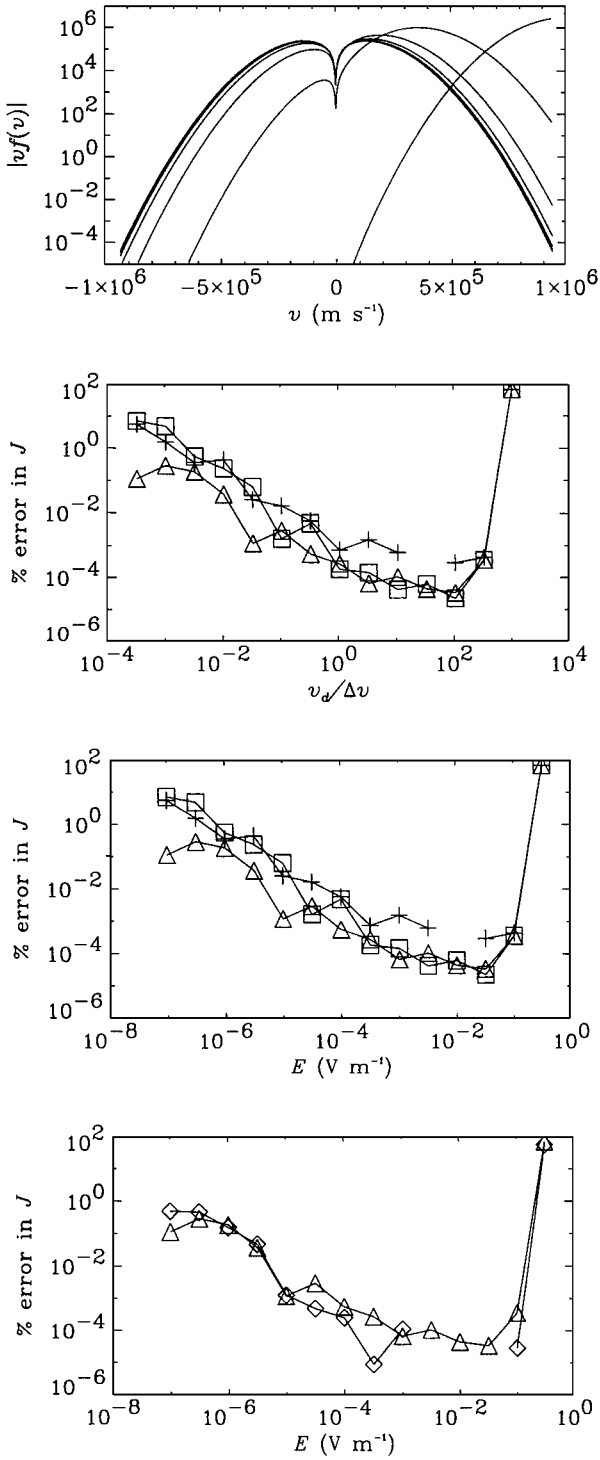

FIG. 2. Comparison between different integration methods for obtaining the current. The top panel shows the function to be integrated for different drift velocities. The middle two panels show the error in the current using Simpson's integration method (crosses), the summing method (squares), and the "in pairs" method (triangles) for 1000 grid points. The bottom panel shows the results of the "in pairs" method when the number of grid points is reduced from 1000 (triangles) to 10 (diamonds).

velocity, and α_e is the thermal velocity defined as $T_e = \frac{1}{2} m_e \alpha_e^2$, where T_e is the electron temperature. In the calculation we set $n_e = 10^6$ m^{-3} and $T_e = 0.1$ eV and vary v_d. The top panel of Fig. 2 shows the flux, vf, versus velocity, v, for 14 different drift velocities. By assuming $E = E_0 \sin(kx - \omega_{pe} t)$, where $\omega_{pe} = (n_e q_e^2/(m_e \epsilon_0))^{1/2}$ is the plasma frequency, and using (5) and (2), the range of v_d corresponds to electric fields in the range $10^{-7} \leq E \leq 5 \times 10^{-1}$ V m^{-1}. The velocity grid has 1000 grid points and the center of the velocity grid is set at $v = 0$ (i.e., calculated at $v = 0$) as the function is zero at this point for all drift velocities. Note however that zero values are not shown on the log scale. The maximum grid velocity, v_{cut}, was set to $v_{cut} = 5\alpha_e$.

The second and third panels show the percentage error in current density versus the drift velocity and electric field, respectively, for the three integration methods. All three methods provide accurate integration for $E \leq 5 \times 10^{-2}$ V m^{-1}. For larger electric fields the function is highly skewed and there is a large contribution to the integral outside $|v_{cut}|$. Tests showed that accuracy could be regained by increasing v_{cut}. Throughout the whole range of drift velocities the "in pairs" method performs consistently better than either the Simpson or summing methods. It is particularly good when compared to the other methods for drift velocities much less than the grid size $v_d/\Delta v \ll 1$. In this region the error in the calculated current is a fraction of a percent while the error in the other methods increases up to 10%. It should also be noted that while the percentage error in J increases with decreasing $v_d/\Delta v$ the absolute error is approximately constant over five orders of magnitude. When the number of points in the "in pairs" method was changed from 1000 to 10 (bottom panel in Fig. 2) it is remarkable that this makes very little difference to the error. This suggests that the first moment of the distribution function is relatively insensitive to the grid resolution when the distribution function is smooth.

LANDAU DAMPING FOR STANDING WAVES

To demonstrate the use and accuracy of the code we now apply it to the Landau damping problem. The electron distribution function is set to be Maxwellian with the same temperature as used above but the initial electron density and drift velocity are allowed to vary in space. We apply a standing wave of the form

$$E = [E_0 \sin(kx - \omega t) + E_0 \sin(kx + \omega t)] e^{\gamma t} \tag{22}$$

to the simulation box, where we assume that the wave is exponentially damped in accordance with linear Landau damping. Here γ is the growth ($\gamma > 0$) or damping ($\gamma < 0$) rate. We solve Poisson's equation to find the electron density variation in space so that at $t = 0$ we have

$$n_e(x) = n_i + \frac{2k\epsilon_0 E_0}{q_e} \cos(kx), \tag{23}$$

where n_i is the constant ion number density and q_e includes the sign of the charge. Solving Ampère's equation, there is a nonzero current at $t = 0$ given by

$$J = -2\gamma \epsilon_0 E_0 \sin(kx), \tag{24}$$

and hence the drift velocity is

$$v_{de}(x) = -\frac{2\gamma\epsilon_0 E_0}{n_e(x)q_e}\sin(kx). \tag{25}$$

The distribution function at $t = 0$ is now defined and is consistent with the long time solution of the Vlasov–Maxwell equations. However, it should be noted that for any perturbation to the Vlasov system there is also a ballistic response which is not included in the long time solution [18]. The ballistic response becomes highly oscillatory in phase space as time increases. Since we do not know what this response would be at $t = 0$, it is omitted from the initial distribution function.

The distribution function having been defined the frequency and damping rate for an initial k for Langmuir waves are found from linear theory [18] as

$$\omega = \omega_{pe}\left(1 + 3k^2\lambda_D^2\right)^{1/2} \tag{26}$$

and

$$\gamma = -\sqrt{\frac{\pi}{8}}\frac{\omega_{pe}}{k^3\lambda_D^3}\exp\left[-\frac{1}{2k^2\lambda_D^2} + \frac{3}{2}\right], \tag{27}$$

where $\lambda_D = \alpha_e/(\omega_{pe}\sqrt{2})$ is the Debye length. To ensure that the physics of Landau damping would be included in the simulation, v_{cut} was set greater than the phase velocity ω/k. We set $v_{cut} = 5\alpha_e$, where the velocity grid extends from $-v_{cut}$ to $+v_{cut}$. We use 300 grid points for the velocity grid so that $\Delta v \ll \alpha_e$. Since it was shown in the last section that the choice of $v_{cut} = 5\alpha_e$ sets a limit on the maximum electric field for accurate integration we choose $E_0 = 0.5$ mV m^{-1} (which gives a maximum electric field of 1 mV m^{-1}) to be well inside that limit.

The boundary conditions for the distribution function are periodic in x and of fourth-order interpolation in v. L is the length of the simulation box in x and is set equal to the wavelength of the applied electric field. The number of spatial grid points is $n_x = 101$; thus the grid resolution satisfies $\Delta x < \lambda_D$. The time step is $\Delta t = 4.96 \times 10^{-7}$ s which corresponds to $a = 1.40 \times 10^{-2}$ and $b = 0.8$. A list of the parameters used in the simulation is given in Table I.

Linear Landau damping is only valid for time scales of the order of the trapping or bounce time for particles in the potential well. The bounce time is given by [5]

$$T_b = 2\pi\sqrt{\frac{m_e}{q_e k E}}. \tag{28}$$

In addition, Vlasov codes with periodic boundary conditions in space are known to have a recurrence effect whereby the particle distribution function at time $t = 0$ is reconstituted (with some small modification) at some later time given by [6]

$$T_r = \frac{2\pi}{k\Delta v}. \tag{29}$$

This corresponds to the time taken for the particles in the lowest velocity grid cell to travel one wavelength back to the same phase on the wave. At the same time, particles

TABLE I
Constants for the Landau Damping Simulations Used in Fig. 3

Quantity	Symbol	Value
Ion number density	n_i	9.0×10^5 m^{-3}
Electron plasma frequency	ω_{pe}	5.352×10^4 rad s^{-1}
Electron temperature	T_e	0.1 eV
Electron thermal velocity	α_e	1.875×10^5 m s^{-1}
Electron drift velocity	v_d	Varies
Debye length	λ_D	2.478 m
Grid length in x	L	5.818×10^1 m
Minimum wavenumber	k_1	0.108 m^{-1}
Number of grid cells in x	n_x	101
Grid cell length in x	Δx	5.818×10^{-1} m
Maximum grid velocity	v_{cut}	$5\alpha_e$
Number of grid cells in v	n_v	301
Grid cell length in v	Δv	6.252×10^3 m s^{-1}
Electric field amplitude	E_0	5.0×10^{-4} V m^{-1}
Courant factor	C_F	0.8
Bounce time	T_b	1.44×10^{-3} s
Recurrence time	T_r	9.31×10^{-3} s
Timestep	Δt	4.96×10^{-7} s

on other velocity grid cells at integer multiples of Δv will have traveled integer multiples of a wavelength and will also be back at the same phase on the wave. Thus a Vlasov simulation of linear Landau damping is only valid on a time scale of T_b or T_r, whichever is the smallest. However, in simulations where the electric field grows to large amplitudes from an initially unstable distribution function the ballistic free streaming trajectories are perturbed and may be trapped by the large electric field. Under these conditions only part of the distribution function in the high velocity grid cells may be reconstituted, if at all, and therefore recurrence should not present a problem.

Figure 3 (top panel) shows an example of the time evolution of the maximum electric field E_{max} for the weakly damped case where $k = 0.108$ m^{-1}. E_{max} is obtained by taking the maximum electric field over the entire simulation box at each time step and therefore oscillates through zero since standing waves are excited in this simulation. Here the waves have no momentum since Poynting's theorem shows there is no energy flux for electrostatic waves. The high-frequency oscillations correspond to oscillations at twice the plasma frequency as expected for electrostatic waves. (Note that a factor of 2 occurs because the waves are standing waves.) The low-frequency envelope corresponds to the bounce frequency and illustrates the effects of linear and nonlinear Landau damping.

Over the first high-frequency cycle E_{max} drops from 1 to approximately 0.78 mV m^{-1}. Exactly the same type of behavior is present in previous simulations (e.g., 6, 20), which solve different equations using numerical schemes different from those presented here. We therefore conclude that this is not a numerical problem. Since linear theory shows that there are two time scales for the plasma to respond to an initial disturbance [18], and that linear Landau damping is only valid on relatively long time scales after the ballistic response has been phase mixed, we attribute the initial drop in E_{max} to initial transient effects, i.e., to the contribution of poles other than the two principal Landau poles [2, 7].

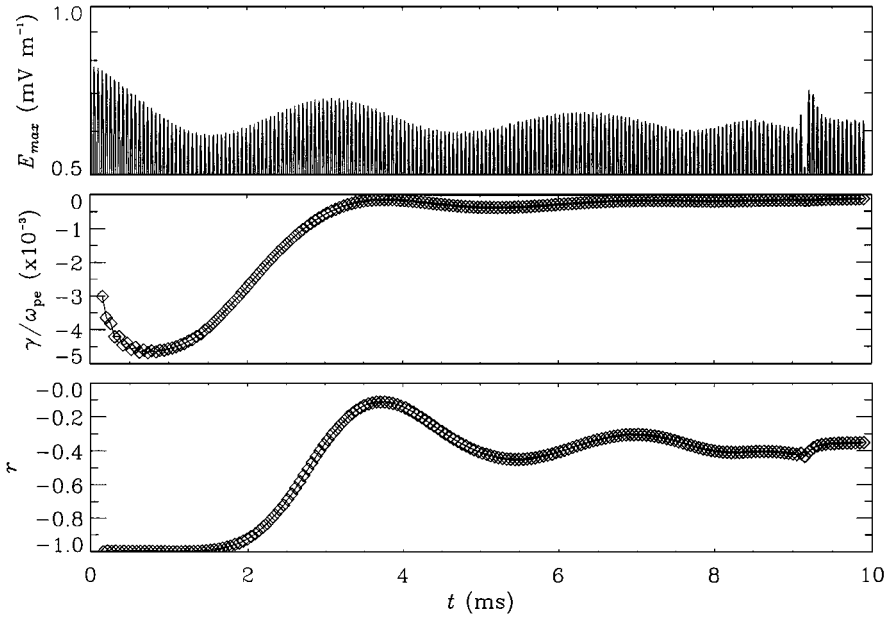

FIG. 3. Weak Landau damping for a standing wave $k = 0.108$ m^{-1}. The time evolution of the maximum electric field E_{max} is shown on a log scale in the top panel. The middle and bottom panels show the damping rate and correlation coefficient obtained from a linear regression through the peaks in the electric field.

Since the electric field should decay exponentially until particles are trapped, we have taken the peaks in $\log(E_{max})$ and calculated the damping rate from a linear regression fit. The first two values of E_{max} have been omitted in the regression analysis to allow for any transient effects to die away. The normalized damping rate, γ/ω_{pe}, is shown in the middle panel of Fig. 3, and the regression correlation coefficient r, which is a measure of how good the fit is, is shown in the bottom panel. Both γ/ω_{pe} and r vary as more and more points are included in the regression analysis. For times less than half the bounce time γ/ω_{pe} varies between -3.0×10^{-3} and -4.7×10^{-3}, and $|r| > 0.997$. This compares with a theoretical value of $\gamma/\omega_{pe} = -6.78 \times 10^{-3}$ using the equations above. The particle bounce time, T_b, corresponds to the breakdown of linear theory. Theoretically we have $T_b = 1.44$ ms which is approximately at the first minimum in the envelope of E_{max}.

The case for smaller wave numbers $k = 0.216$ m^{-1} where Landau damping is stronger is shown in Fig. 4. The electric field decays by more than three orders of magnitude down to an almost constant minimum level. The recurrence effect is quite clearly seen close to the theoretical value of $t = 4.65$ ms where the electric field is reconstituted. The electric field does not reach its original value because of effects other than free streaming. The recurrence effect is a numerical effect introduced by a finite velocity grid. In the analytical limit, $\Delta v \to 0$, this effect would not be present. However, the recurrence effect can be regarded as another way of demonstrating the concept of phase memory and therefore a test of the simulation code. The theory of Landau damping shows that, while the electric field may decay down to the noise level, the particles retain information about the initial disturbance in a collisionless plasma. The concept has been demonstrated experimentally in the laboratory through the phenomenon of plasma wave echoes [22]. In our simulation phase memory is stored in the velocity distribution function. As information propagates through the spatial

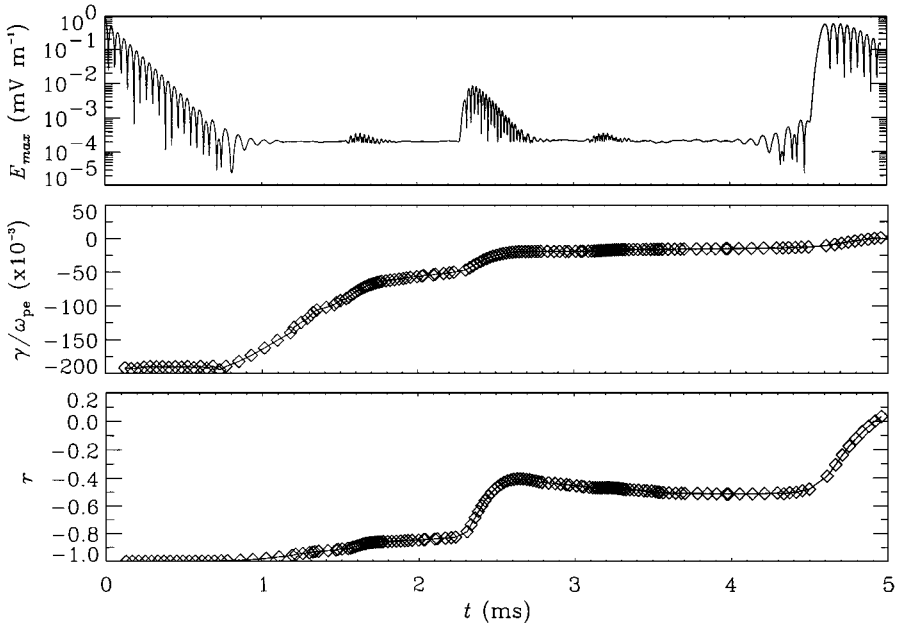

FIG. 4. Strong Landau damping for a standing wave $k = 0.216$ m^{-1}. Here $\Delta t = 2.48 \times 10^{-7}$ s, $T_b = 1.02 \times 10^{-3}$ s, and $T_r = 4.65 \times 10^{-3}$ s.

grid at different velocities, periodic boundary conditions in space ensure that at some later time, T_r, information on the velocity grid will end up back in phase after information in the lowest grid cell has traveled an integral number of wavelengths, thus reconstituting the initial disturbance. The recurrence effect demonstrates that our simulation code retains the property of phase memory. In some simulation codes the distribution function is smoothed to eliminate high-frequency oscillations on the velocity grid [e.g., 15], often referred to as filamentation. Smoothing may not only remove the recurrence effect, but also eliminate phase memory, which is a real physical effect.

A comparison between the linear Landau damping rates obtained from our Vlasov simulations and those from linear theory is shown in Fig. 5. The solid line shows the damping rates obtained from numerical solutions of the linear dispersion relation using the HOTRAY code [12] and the dashed line shows the analytical results using Eqs. (26) and (27). The diamonds show the Vlasov simulation results derived from the linear regression of $\log(E_{max})$ on t for $t < T_b/2$. No results are shown for $k\lambda_D > 0.6$ since the HOTRAY code cannot converge on a solution, and since it becomes very difficult to determine the damping rate from the Vlasov simulation due to the very rapid decay of the wave electric field. The Vlasov simulation results agree extremely well with the HOTRAY results, rather than the analytical result, for all $k\lambda_D$ shown. Thus, even though the simulation code uses the damping rate from analytical theory to initiate the run, which may be in error, the damping rate calculated from the output is correct.

LANDAU DAMPING FOR TRAVELING WAVES

We now consider the case of a traveling wave in the simulation box of the form

$$E = E_0 \sin(kx - \omega t)e^{\gamma t}. \tag{30}$$

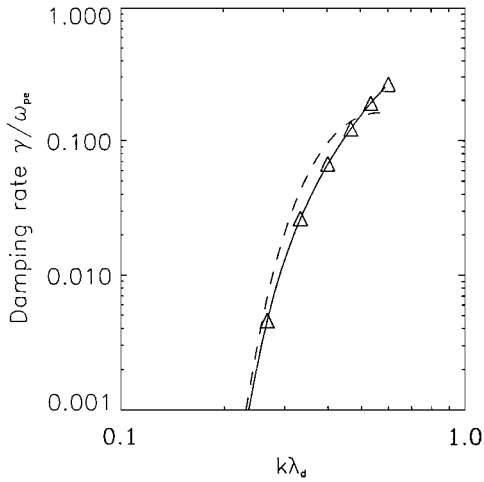

FIG. 5. Comparison between the damping rates obtained from theory (dashed line), numerical solutions of the linear dispersion relation using HOTRAY (solid line), and the Vlasov simulation code for standing waves (triangles).

Solving Poisson's equation we obtain the electron density at $t = 0$ as

$$n_e(x) = n_i + \frac{k\epsilon_0 E_0}{q_e}\cos(kx). \tag{31}$$

and solving Ampère's equation we obtain a current at $t = 0$ given by

$$J = \epsilon_0 E_0(\omega\cos(kx) - \gamma\sin(kx)), \tag{32}$$

and hence the drift velocity in the Maxwellian distribution at $t = 0$ is

$$v_{de}(x) = \frac{\epsilon_0 E_0}{n_e(x)q_e}(\omega\cos(kx) - \gamma\sin(kx)). \tag{33}$$

The results for Landau damping of a traveling wave with $k = 0.243$ m^{-1} are shown in Fig. 6 for the same plasma parameters as before. The top panel shows the results for initial values of ω and γ taken from analytical theory. Instead of E_{max} decaying smoothly there is now a ripple on the electric field. Even when the exact numerical solutions for ω and γ are provided as input (middle panel), or when $\gamma = 0$ (bottom panel), there is very little effect on the ripple. In fact we find that the decay rate is very robust in a wide range of ω and γ but that the initial value of ω effectively controls the amplitude of the ripple. We interpret the ripple as being due to a standing wave being excited on top of the traveling wave. Since $\Delta E_{max}/E_{max}$ remains approximately constant in time this suggests that both waves decay at the same rate and therefore have the same wavelength. We believe that the ripple originates from the initial transient effects, i.e., due to the contribution of poles other than the two principal Landau poles which are not included in the initial conditions (Eqs. (30)–(33)).

Although the presence of an additional standing wave does not affect our linear Landau damping results, its presence in other applications may be important. For example, in the transmitter problem one needs to know how electric fields transmitted from a spacecraft

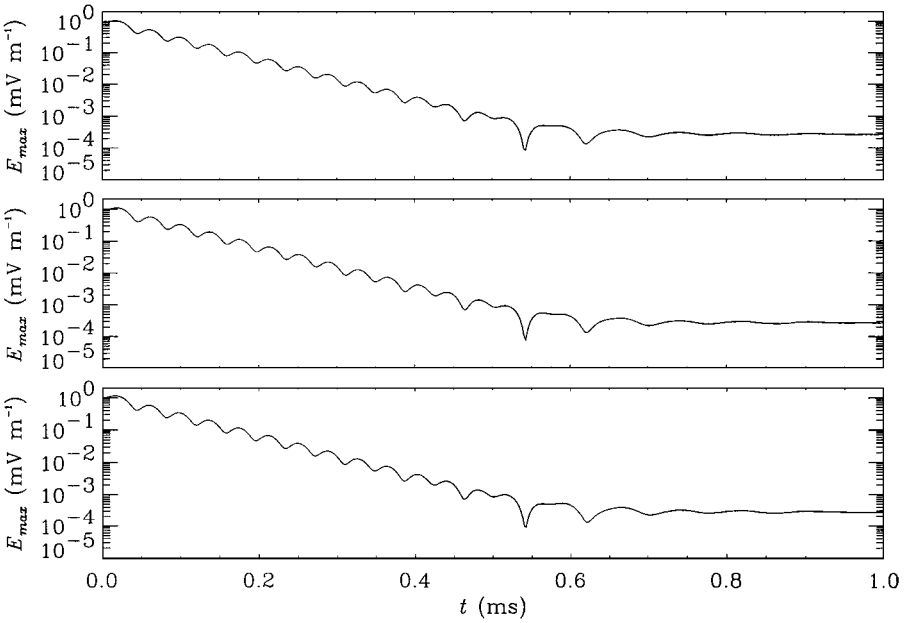

FIG. 6. Strong Landau damping for a traveling wave $k = 0.243$ m^{-1}. The results are shown for theoretical input values of ω and γ (top), numerical solutions using HOTRAY (middle), and numerical solutions for ω but $\gamma = 0$ (bottom). Here $\Delta t = 2.21 \times 10^{-7}$ s, $T_b = 9.61 \times 10^{-4}$ s, and $T_r = 4.14 \times 10^{-3}$ s.

couple to the plasma. If both propagating and standing waves are excited, as our simulations suggest, then this may lead to additional nonlinear scattering from the standing waves and a more complicated coupling mechanism.

TRAVELING VERSUS STANDING WAVES

By solving the Vlasov–Ampère equations both standing and traveling waves can be obtained depending on the initial current. If the initial current is zero, we obtain standing waves; if it is nonzero we obtain traveling waves. (Note that in Figs. 3 and 4 the initial current is very small which is why the result is a standing wave.) However, in a version of our code where we solve the Vlasov–Poisson equations for periodic boundary conditions standing wave solutions were obtained even when the initial current was nonzero. The difference is due to the method of calculating the electric field. When using Poisson's equation the field at one position must be specified in order for the field across the grid to be calculated. For a standing wave one can choose $E = 0$ at the boundary. However, for a traveling wave it is not clear what value to choose at the boundary, or at which location the field should be zero on subsequent time steps. Since some choice must be made, the easiest solution is to set the field to be a constant value at the boundary which results in a standing wave. In contrast, in solving Ampère's equation the electric field is obtained from the current and a previous value of the electric field at the same location. The field does not need to be specified at the boundary and thus traveling wave solutions are possible with the Vlasov–Ampère equations. However, we note that it may also be possible to obtain traveling wave solutions in other Vlasov–Poisson codes by choosing an initial distribution function that preferentially damps traveling waves propagating in one direction [13].

ELECTRON TRAPPING

We have also tested the code for the case where the initial energy density of the wave (1.1×10^{-14} J m^{-3}) is comparable to the energy density of the thermal electrons (1.4×10^{-14} J m^{-3}) to see if the numerical scheme can cope with the effects of particle trapping. Figure 7 (top panel) shows the evolution of the electric field for a much larger initial E field of 50 mV m^{-1} and wavenumber $k = 0.162$ m^{-1}. The number of grid cells is the same as before, but now the timestep determined from the stability criteria is $\Delta t = 3.31 \times 10^{-7}$ s and the bounce time ($T_b = 1.66 \times 10^{-4}$ s) is less than the recurrence time ($T_r = 6.20 \times 10^{-3}$ s). The initial decay of the electric field and subsequent increase at about $t \approx T_b$ indicates that particle trapping in the potential well of the wave is taking place. The linear regression fit through the maxima of the electric field is shown in the middle panel. Note that the first point corresponds to a fit through the first three maxima where $t < T_b$ and yields a damping rate $\gamma/\omega_{pe} < -0.35$. This is much higher than the linear damping rate at this value of k (see Fig. 5) indicating nonlinear Landau damping.

To illustrate trapping effects more clearly, plots of the distribution function are shown in Fig. 8. Note that for clarity the surface plots in the left-hand column show the log of the distribution function for one half of the velocity grid while the contour plots in the right-hand column show both positive and negative velocities. The distribution function in the top panel is shown for $t = 4.47 \times 10^{-4}$ s, such that $T_b < t < T_r$, with time increasing down the page. Electron trapping can be identified in the distribution function by the elliptical depression in the surface plot at a velocity centred at approximately $\pm 4.0 \times 10^5$ m s^{-1}. This value corresponds very well to the phase velocity of the wave calculated from (26). The

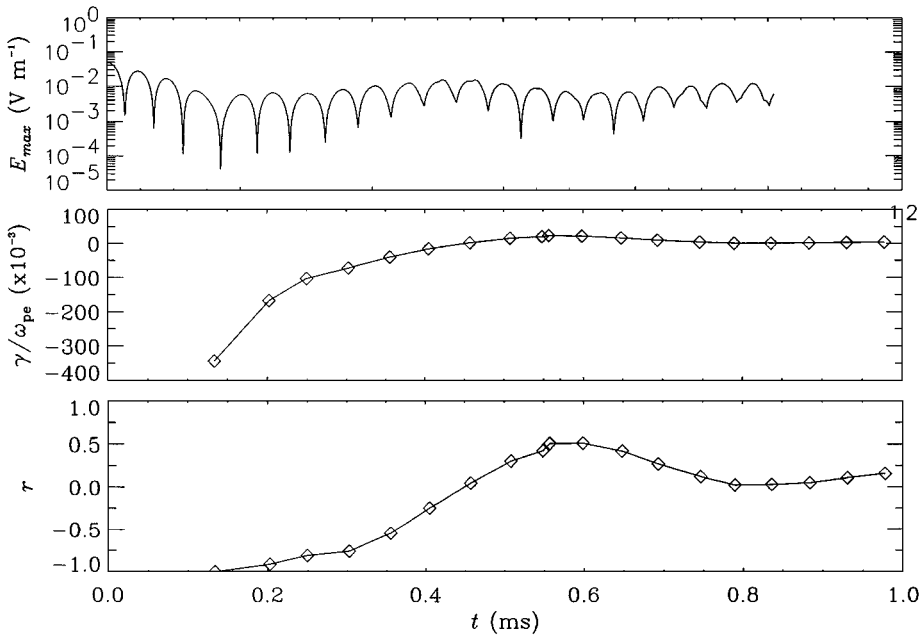

FIG. 7. Nonlinear Landau damping for a standing wave with $k = 0.162$ m^{-1} and $E = 50$ mV m^{-1}. The time evolution of the maximum electric field E_{max} is shown on a log scale in the top panel. The middle and bottom panels show the damping rate and correlation coefficient obtained from a linear regression through the peaks in the electric field. The first point in the middle panel corresponds to a fit through the first three maxima.

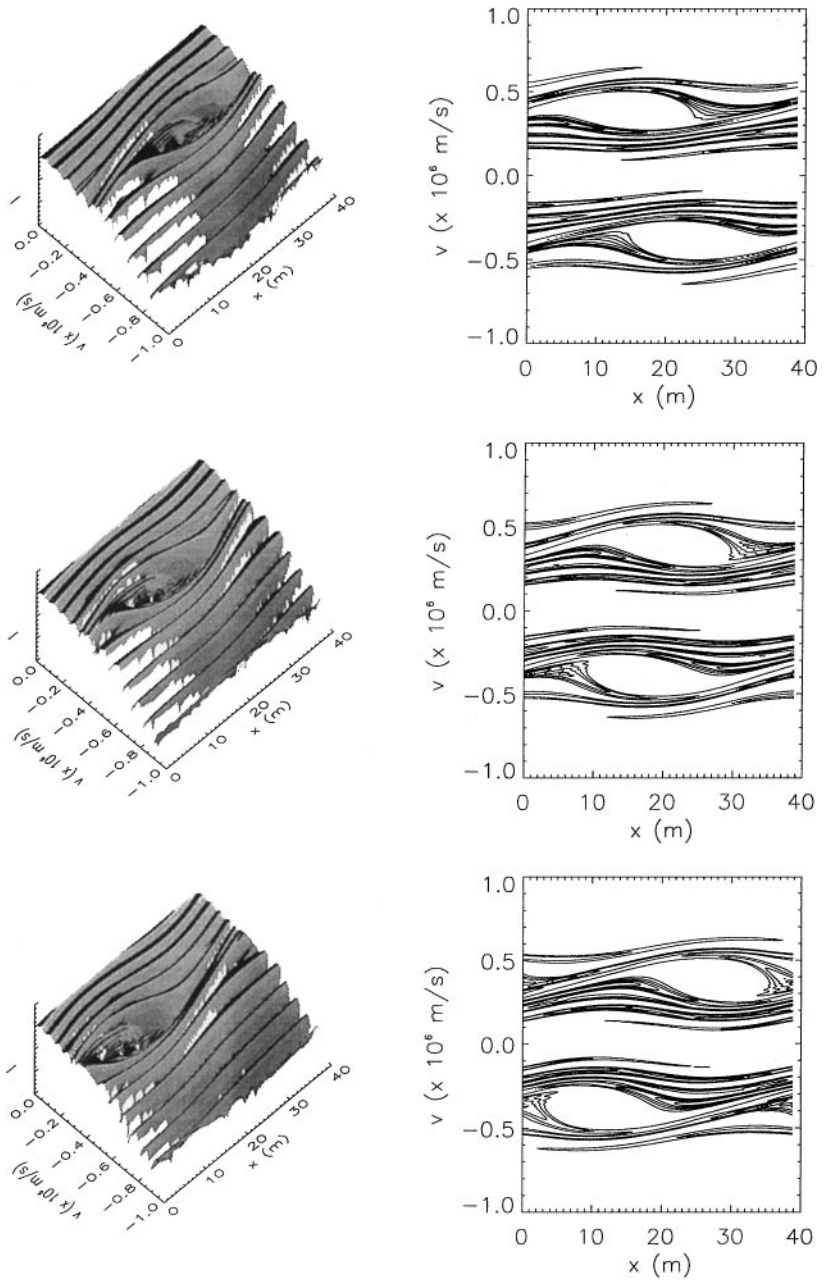

FIG. 8. The electron distribution function for three selected times illustrating electron trapping effects. The surface plots (left-hand column) show the log of the distribution function for one half of the velocity grid only. The contour plots (right-hand column) illustrate left and right going waves constituting a standing wave. Time evolves down the page from $t = 4.47$, 4.63, and 4.80×10^{-4} s.

contour plots show the presence of two regions of trapping, corresponding to waves traveling in opposite directions, as expected for a standing wave. The structure in the distribution function outside the region of trapping is caused by filamentation. Note that as the time sequence evolves from 4.47 to 4.80×10^{-4} s the elliptical structures maintain their form and move across the simulation grid as required. Thus, at least for this set of parameters, the

code can reproduce the results of particle trapping. However, we note that the application of smoothing techniques (e.g., 14) may be required for some scientific problems but this is left for a future development.

CONCLUSIONS

We have developed a new numerical simulation code for electrostatic waves in one dimension. To our knowledge, the code is unique in that it solves the Vlasov–Ampère equations and not the Vlasov–Poisson equations as used in previous simulation codes. The advantage of using Ampère's equation is that no spatial boundary conditions are required for integration of the electric field and the code should be extendable to electromagnetic waves as well. The Vlasov equation is integrated forward using MacCormack's method, which does not depend on a splitting scheme used in previous Vlasov simulation codes and is second-order accurate but does not require second-order derivatives to be calculated explicitly. We found MacCormack's method easy to implement and reliable. We have also demonstrated a simple and accurate method of integrating the distribution function to obtain the current. Our stability analysis applied to the Vlasov–Ampère equations yielded two necessary conditions on the time step. One is the usual CFL condition for the linear spatial advection equation; the other is an equivalent CFL condition for advection on the velocity grid. However, satisfying both these conditions is not sufficient for stability. Instead, we have shown that there is a simple linear relation between the two conditions which does guarantee stability.

In our application to Landau damping, the results are in excellent agreement with numerical solutions of the linear dispersion relation over a wide range of $k\lambda_D$ where the growth rates are small. The code retains phase memory after the electric field has decayed, as demonstrated by the recurrence effect. The code can also reproduce the effects of nonlinear trapping. Solving the Vlasov–Ampère equations allows both standing and traveling wave solutions depending on the initial current, whereas in solving the Vlasov–Poisson equations one must know how to set the boundary conditions on E in Poisson's equation in order to obtain traveling waves for periodic boundary conditions. Finally we point out that even though Maxwell's equations may be satisfied for traveling waves initially, additional standing waves may be set up in the simulation. This may be important in simulations designed to study how wave fields from a transmitter embedded in a plasma couple to the plasma.

ACKNOWLEDGMENTS

We thank Caroline van Heusden and Kelvin Wu for their help during the initial part of this work and the Natural Environment Research Council for providing the necessary computing facilities.

REFERENCES

1. J. D. Anderson, Jr., Explicit finite difference methods: Some selected applications to inviscid and viscous flows, *Computational Fluid Dynamics: An Introduction*, edited by John F. Wendt (Springer-Verlag, Berlin, 1992), Chap. 7, p. 123.
2. P. Bertrand and M. R. Feix, *Plasma Phys.* **20**, 1075 (1978).
3. J. A. Byers and J. Killeen, Finite difference methods for collisionless plasma models, in *Methods in Computational Physics*, Plasma Physics (Academic Press, New York, 1970), Vol. 9, p. 259.

4. G. Chanteur, Vlasov simulations of ion acoustic double layers, *Computer Simulation of Space Plasmas*, edited by H. Matsumoto and T. Sato (Terra Scientific Publishing Company, Tokyo, 1984), p. 279.
5. F. F. Chen, *Introduction to Plasma Physics and Controlled Fusion* (Plenum, New York, 1990), Vol. 1, p. 329.
6. C. Z. Cheng and G. Knorr, The integration of the Vlasov equation in configuration space, *J. Comput. Phys.* **22**, 330 (1976).
7. J. Denavit, *Phys. Fluids* **2**, 680 (1968).
8. J. Denavit, *J. Comput. Phys.* **9**, 75 (1972).
9. J. Denavit, *Phys. Fluids* **28**(9), 2773 (1985).
10. J. Gazdag, Numerical solution of the Vlasov equation with the accurate space derivative method, *J. Comput. Phys.* **19**, 77 (1975).
11. F. C. Grant and M. R. Feix, Fourier–Hermite solutions of the Vlasov equation in the linearized limit, *Phys. Fluids* **10**(4), 696 (1967).
12. R. B. Horne, Path-integrated growth of electrostatic waves: The generation of Terrestrial Myriametric Radiation, *J. Geophys. Res.* **94**, 8895 (1989).
13. T. W. Johnston, P. Bertrand, A. Ghizzo, M. Shoucri, E. Fijalkow, and M. R. Feix, Stimulated Raman scattering: Action evolution and particle trapping via Euler–Vlasov fluid simulation, *Phys. Fluids B* **4**(8), 2523 (1992).
14. A. J. Klimas, A method for overcoming the velocity space filamentation problem in collisionless plasma model solutions, *J. Comput. Phys.* **68**, 202 (1987).
15. A. J. Klimas and W. M. Farrell, A splitting algorithm for Vlasov simulation with filamentation filtration, *J. Comput. Phys.* **110**, 150 (1994).
16. A. J. Klimas and J. Cooper, Vlasov–Maxwell and Vlasov–Poisson equations as models of a one-dimensional electron plasma, *Phys. Fluids* **26**, 478 (1983).
17. A. J. Klimas Vlasov simulation with filamentation removed, *STEP SIMPO Newsletter* **5**, 7 (1995).
18. N. A. Krall and A. W. Trivelpiece, *Principles of Plasma Physics* (McGraw-Hill, Tokyo, 1973), Chaps. 9 and 10, p. 442.
19. D. Nunn, A novel technique for the numerical simulation of hot collision-free plasma: Vlasov hybrid simulation, *J. Comput. Phys.* **108**, 180 (1993).
20. J. W. Schumer and J. P. Holloway, Vlasov simulations using velocity-scaled Hermite representations, *J. Comput. Phys.* **144**, 626 (1998).
21. H. Ueda, Y. Omura, H. Matsumoto, and T. Okuzawa, A study of the numerical heating in electrostatic particle simulations, *Comput. Phys. Commun.* **79**, 249 (1994).
22. A. Y. Wong and D. R. Baker, *Phys. Rev.* **188**, 326 (1969).